Supporting information

Amorphous Trimetallic (Ni-Co-Fe) Hydroxides Sheathed 3D Bifunctional Electrode for Superior Oxygen Evolution and High Performance Cable-type Flexible Zinc-air Batteries

Simeng Li [a], Xuhuan Yang [a], Siyuan Yang [a], Qiongzhi Gao [a], Shengsen Zhang [a], Xiaoyuan Yu [a], Yueping Fang* [a,d], Shihe Yang* [b,c], Xin Cai* [a,d]

[a]*College of Materials and Energy, South China Agricultural University, Guangzhou, Guangdong 510642, China. E-mail: caixin2015@scau.edu.cn; ypfang@scau.edu.cn*

[b]*Guangdong Key Lab of Nano-Micro Material Research, School of Chemical Biology and Biotechnology, Shenzhen Graduate School, Peking University, Shenzhen, China*

[c]*Department of Chemistry, The Hong Kong University of Science and Technology, Clear Water Bay, Kowloon, Hong Kong (China). E-mail: chsyang@pku.edu.cn*

[d]*Guangdong Laboratory for Lingnan Modern Agriculture, South China Agricultural University, Guangzhou, Guangdong 510642, People's Republic of China*

Experimental Section

Synthesis of NiCo$_2$O$_4$ nanowires and NiCo$_2$O$_4$@NiCoFe-OH nanoarrays on carbon cloth (CC)

A piece of carbon cloth (2 × 5 cm^2, W0S1009, Cetech) was initially treated by concentrated nitric acid at 90℃ for 5 h, thoroughly rinsed with deionized water and vacuum dried for use. To grow NiCo$_2$O$_4$ nanowires (NWs) on CC, 2 mmol cobalt (II) nitrate hexahydrate, 1 mmol nickel (II) nitrate hexahydrate, and 12 mmol urea were sufficiently dissolved into a mixed solvent including 35 mL of ethanol and deionized water (*v/v*=1:1), and then magnetically stirred. The formed uniform pink dispersion was shifted into a Teflon-lined autoclave (50 mL) with vertical immersion of the CC substrate in the reaction system, which was kept at 100℃ for 12 h. The received piece was thoroughly washed by deionized water, dried and annealed at 350 °C in air for 2 h with a heat rate of 5 °C min^{-1}, crystallized NiCo$_2$O$_4$ nanowires (NWs) were established on CC (the membrane electrode is denoted as NiCo$_2$O$_4$). As for the preparation of NiCo$_2$O$_4$@NiCoFe-OH, 4 mmol of nickel (II) nitrate hexahydrate, 2 mmol of cobalt (II) nitrate hexahydrate and 3 mmol iron(III) nitrate nonahydrate were well dispersed in a co-solvent mixture containing 66 ml 1-methyl-2-pyrrolidone (NMP) and 5 mL deionized water. 35 mL of such dispersion was put in a 50 mL Teflon-lined autoclave, after which above NiCo$_2$O$_4$ coated CC vertically placed in the mixture and endured a 6 h-thermal reaction at 180 ℃. The as-collected piece was finally washed by deionized water and dried, producing the NiCo$_2$O$_4$@NiCoFe-OH nanoarrays on CC (the membrane electrode is denoted as NiCo$_2$O$_4$@NiCoFe-OH). For comparison, NiCoFe-

OH electrode was fabricated under the same condition by direct growth of NiCoFe-OH film onto CC substrate without $NiCo_2O_4$ NWs.

Materials characterization

Field-emission scanning electron microscope (SEM, Merlin, Zeiss), Transmission electron microscope (TEM, Philips-FEI Tecnai G2S-Twin microscope, 200 kV accelerating voltage) were used to image the microstructure and morphology of the different catalysts. X-ray diffraction (XRD) patterns were recorded on a Rigaku D/Max 2550 X-ray diffractometer with Cu Kα radiation. X-ray photoelectron spectroscopy (XPS, VG ESCALAB250) was used to analyze the surface properties of the samples.

Electrochemical measurement

The electrochemical activities of the binder-free catalytic electrode were studied on a CHI electrochemical workstation (760E, China) through a typical three-electrode system. CC covered with electrocatalysts directly played as the working electrode, Ag/AgCl acted as the reference electrode and Pt plate was employed as the counter electrode, respectively. OER activities were tested in 1 M KOH electrolyte and ORR was performed by using 0.1 M KOH solution under O_2-saturated condition. Electrochemically active surface area (ECSA) was obtained from cyclic voltammetry (CV) curves ranging from 0 to 0.1 V versus Ag/AgCl in 1 M KOH aqueous solution, adopting scan rates from 3 to 15 mV s^{-1}. All the recorded potentials were calibrated to the RHE on the basis of the equation as follows:

$$E_{(RHE)} = E_{(Ag/AgCl)} + E^0_{(Ag/AgCl, 0.199)} + 0.0591\text{pH} \tag{1}$$

RuO$_2$ loaded on CC (RuO$_2$): Commercial RuO$_2$ powder (5 mg, Aladdin) and XC-72 (1 mg) were dispersed in 1 mL ethanol mixture containing 50 μL Nafion solution (5 wt.%). The mixture was ultra sonicated for 60 min to produce a homogeneous dispersion. The dispersion was drop-casted onto a pretreated CC substrate (1×1.3 cm^2). The loading mass of RuO$_2$ was kept in line with the as-prepared samples of 1.2 mg cm^{-2}. The preparation of Pt/C electrode was basically the same as the RuO$_2$ electrode except that commercial Pt/C catalyst (5 mg, 20 wt.%, Macklin) was used.

Fabrication and characterization of the aqueous rechargeable ZABs

The aqueous ZABs were constructed by employing a 300 μm thick zinc foil as the anode, the free standing NiCo$_2$O$_4$@NiCoFe-OH electrode directly as the air cathode (geometric area: 1×1 cm^2) and 6 M KOH-based electrolyte containing 0.2 M zinc acetate as the additive. All the mentioned ZABs in this study were measured under air condition (i.e., capturing O$_2$ from the air) at room temperature. Electrochemical measurements of the as-fabricated batteries were proceeded on an electrochemical workstation (CHI 760E) and a NEWARE battery system (CT-3008). The specific discharge capacity (mA h g$_{zinc}^{-1}$) and gravimetric energy density (mW h g$_{zinc}^{-1}$) of the batteries were calculated via following equations, respectively.

$$Specific\ capacity = \frac{Discharge\ current\ \times time}{Weight\ of\ consumed\ zinc} \tag{2}$$

Gravimetric energy density

$$= \frac{Discharge\ current\ \times time\ \times average\ dicharge\ voltage}{Weight\ of\ consumed\ zinc} \tag{3}$$

Assembly and characterization of the cable-type ZABs

Firstly, 5 mL of mixed 11.25 M KOH and 0.25 M ZnO was fabricated. Then, 0.5 g of acrylic acid and 0.075 g of N, N'-methylene-bisacrylamide were added into the former solution and stirred vigorously. The white sediment was successively filtered out to acquire a settled solution, marked as solution A, and 3 M $K_2S_2O_4$ aqueous solution was prepared as solution B ready for use. Typically, 75 µL solution B was dropwise mixed with solution A under vigorous agitation. The as-prepared mixture was carefully poured onto a culture dish. The generated transparent film was peeled off and used as the thin gel film. Then, a zinc wire (diameter: 1 mm) was densely winded onto a metal rod (diameter: 2 mm) and taken out to produce the helical/spiral anode. The above-received film acted as the gel electrolyte and was carefully wrapped onto the Zn spring, and consequently the $NiCo_2O_4$@NiCoFe–OH cathode was wound around the gel film covered zinc anode. Finally, heat shrinkable tube with tailored holes as the packaging film was adopted to encapsulate the cable battery. The galvanostatic charge/discharge measurements were performed on the CHI 760E electrochemical workstation. The charge/discharge polarization curves of the batteries were recorded by liner sweep voltammetry measurements at 10 mV s^{-1}. Rate capability was evaluated under varied current densities from 1 to 12 mA cm^{-3} through NEWARE CT-3008 battery testing system. Noting that the relevant current densities had been normalized to the volume of the cable-type ZAB. Electrochemical impedance spectroscopy (EIS) was implemented across the frequency of 0.01 Hz-100 kHz under the open circuit potential

condition. According to the galvanostatic discharge curves of the cable-type ZAB at 2.2 mA cm^{-3}, the corresponding volumetric energy density (mW h cm^{-3}) was calculated by the following formula. Noting that the calculated volume covering the entire volume of the basic components within batteries.

Volumetric energy density

$$= \frac{Discharge\ current\ \times\ time\ \times average\ discharge\ voltage}{Volume\ of\ zinc\ air\ battery} \quad (4)$$
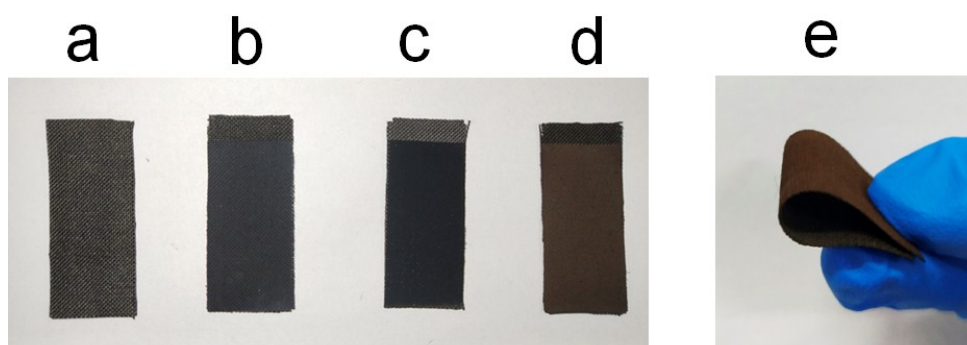
Figure S1 Optical photo of the samples. (a) carbon cloth (CC); (b)NiCo precursor coated CC; (c) CC/NiCo$_2$O$_4$ nanowires; (d), (e)CC/NiCo$_2$O$_4$@NiCoFe-OH.
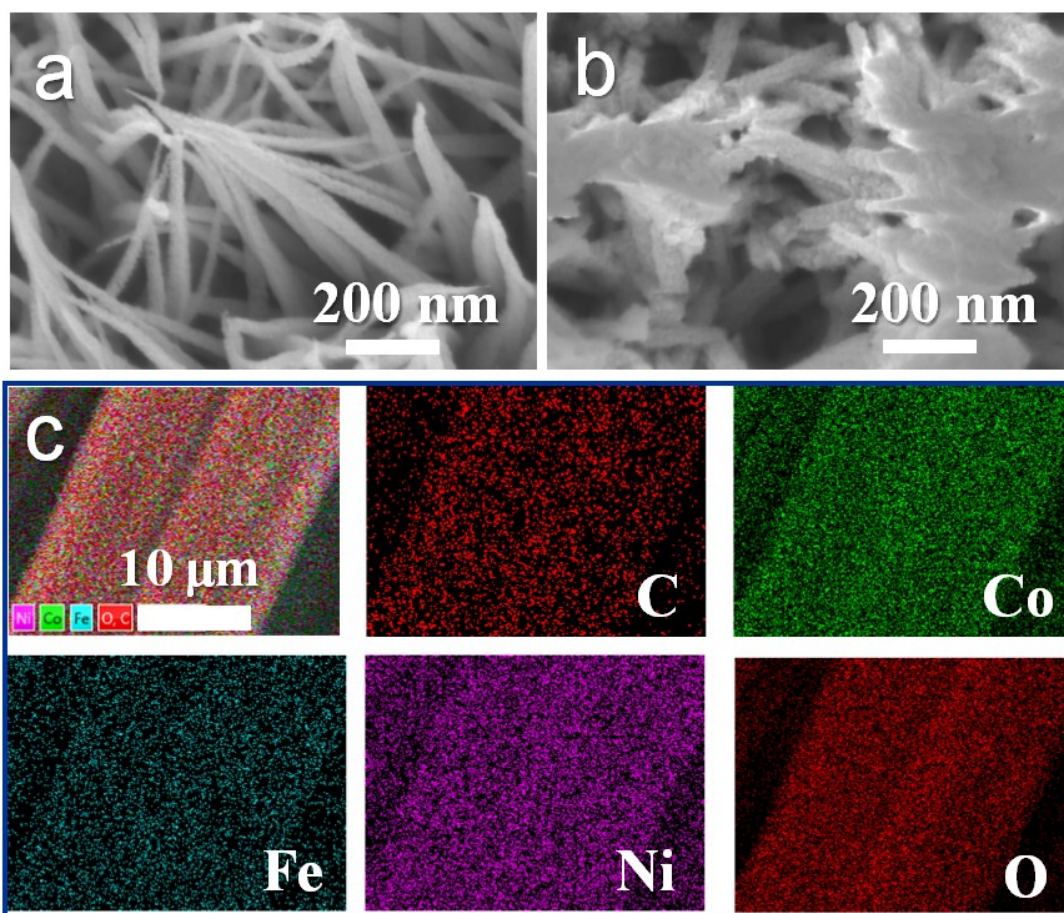
Figure S2 (a) SEM image of NiCo$_2$O$_4$ nanowires grown on CC; SEM image (b) and energy dispersive X-ray spectroscopy (EDS) mapping images (c) of NiCo$_2$O$_4$@NiCoFe-OH.
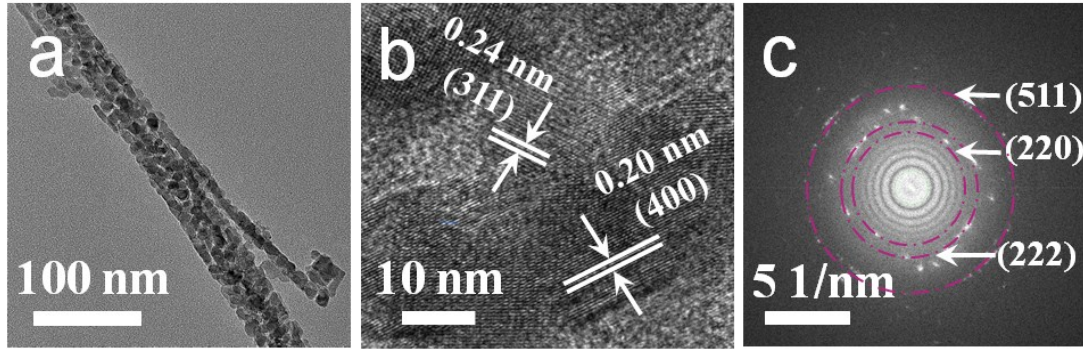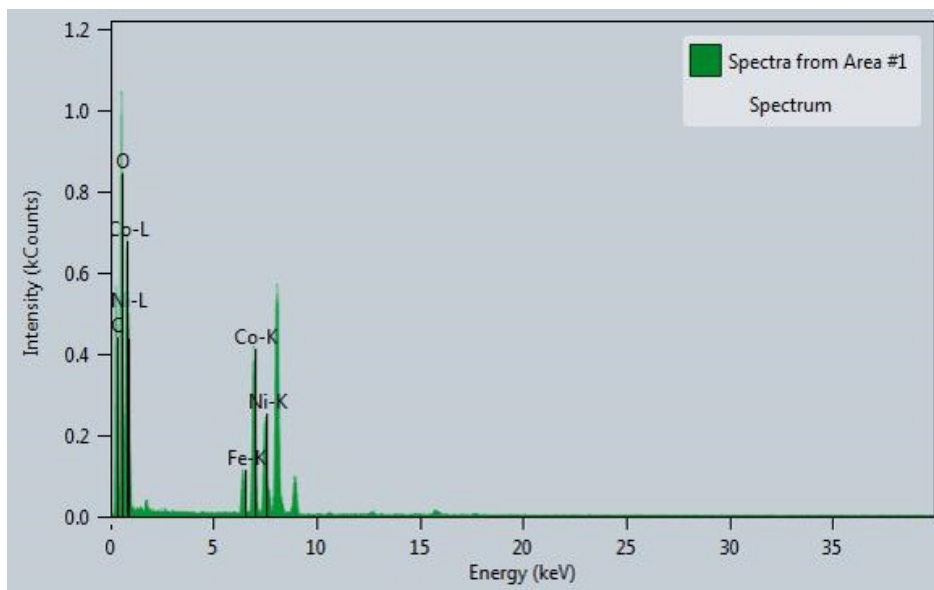
Figure S3 (a), (b) HR-TEM images of NiCo$_2$O$_4$; (c) Fast Fourier Transform image of NiCo$_2$O$_4$.
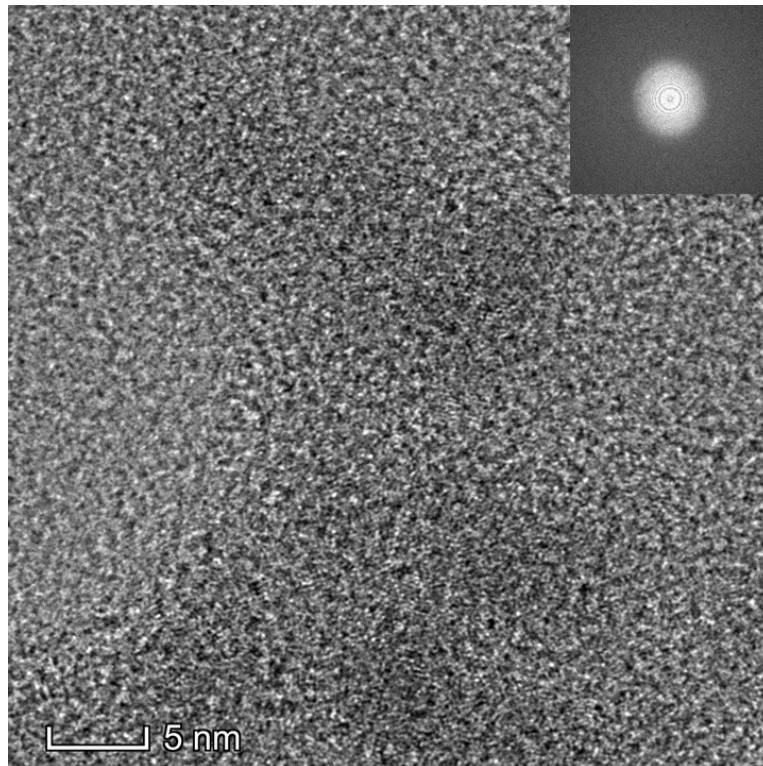
**Figure S4** HR-TEM and corresponding Fast Fourier Transform (FFT) image (inset) of NiCoFe-OH.

No obvious and characteristic lattice fringes are identified for the NiCoFe-OH sample. Also, the diffused diffraction halo in the FFT image further indicates the amorphous feature of NiCoFe-OH.
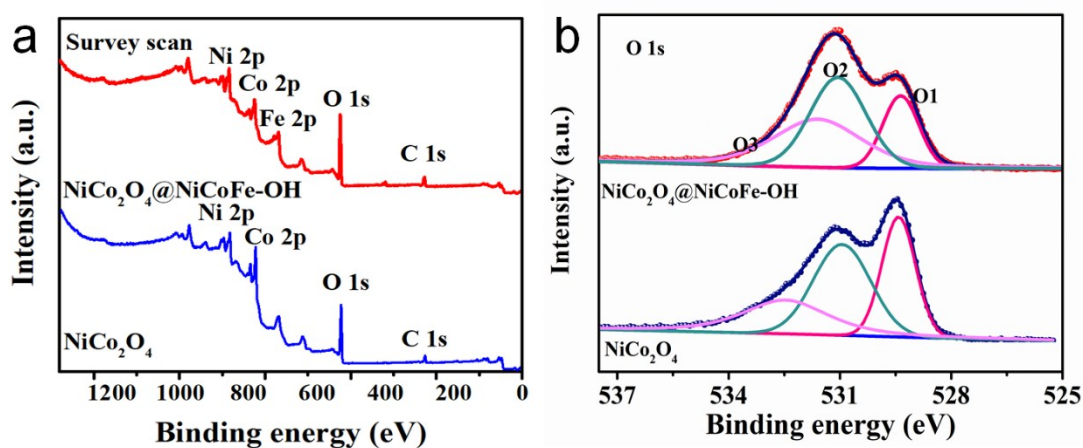
Figure S5 EDS spectrum of $NiCo_2O_4$@NiCoFe-OH.

Table S1 Elemental composition of the as-prepared $NiCo_2O_4$@NiCoFe-OH sample by EDS analysis.

Element	Atomic Fraction (%)	Mass Fraction (%)
C	37.51	18.65
O	39.73	26.31
Fe	3.17	7.33
Co	11.97	29.19
Ni	7.63	18.53
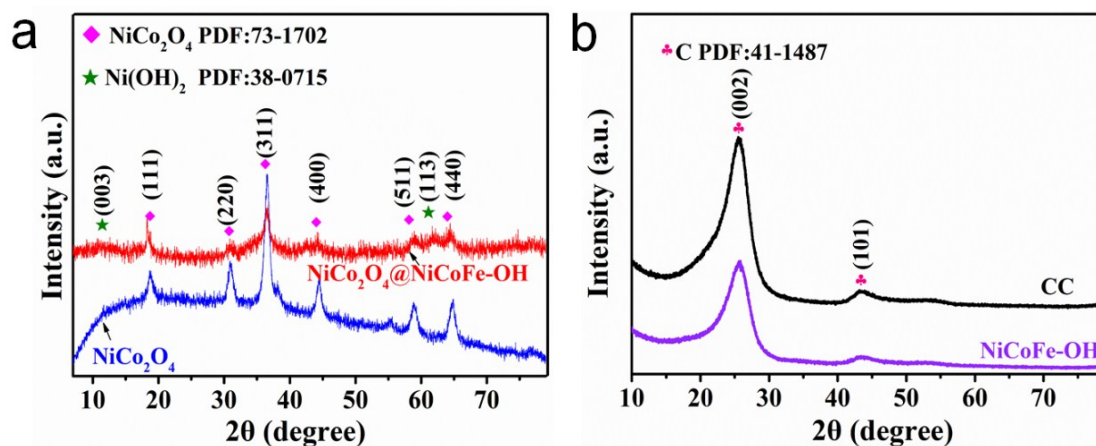
**Figure S6** (a) XRD pattens of $NiCo_2O_4$ and $NiCo_2O_4@NiCoFe-OH$, respectively. (b) XRD patterns of NiCoFe-OH and pure carbon cloth (CC).

Figure S7 (a) XPS survey spectra of $NiCo_2O_4$ and $NiCo_2O_4@NiCoFe-OH$, respectively. (b) O1s spectra.

Table S2 The electrocatalytic activities of recently reported NiCo oxides and ternary electrocatalysts for OER.

Catalysts	Electrolyte	Loading (mg cm^{-2})	Overpotential (mV vs. RHE) at 10 mA cm^{-2}	Onset overpotential (mV vs. RHE)	Endurance (Current retention)	Ref.
NiCo$_2$O$_4$@ NiCoFe-OH	1.0 M KOH	1.02	235	178	99.6% (36 h)	This work
(Ni$_2$Co$_1$)$_{0.925}$ Fe$_{0.075}$-MOF-Ni foam	1.0 M KOH	0.54	257	----	93% (35 h)	[S1]
Ni$_2$Co^{III}Fe-LDH/N-GO	0.1M KOH	0.085	317	180	90 % (8.3 h)	[S2]
CoNiMn-LDH/PPy/RGO	1.0 M KOH	0.2	369	230	89.7 % (5 h)	[S3]
FeCoNi oxynitride	1.0 M KOH	0.284	291	230	----	[S4]
Ni$_x$Co$_y$O$_4$/ Co-N-rGO	0.1 M KOH	0.2	400	230	----	[S5]
NiCo/NiCoO$_x$ nanowire arrays@Ni foam	1.0 M KOH	0.7	360	270	----	[S6]
NiCo$_2$O$_4$ nanosheets	1.0 M KOH	0.285	320	300	----	[S7]
Co$_3$O$_4$/NiCo$_2$O$_4$ nanocages	1.0 M KOH	1.0	340	300	96% (10 h)	[S8]
NiCo$_2$O$_4$@NiMn LDH	1.0 M KOH	2.0	255	216	96% (20 h)	[S9]

| NiCo$_2$O$_4$@ N-OCNT	1.0 M KOH	0.71	270	220	----	[S10]
Ni-doped CoFe$_2$O$_4$ nanospheres	0.1 M KOH	0.4	340	----	100% (12 h)	[S11]
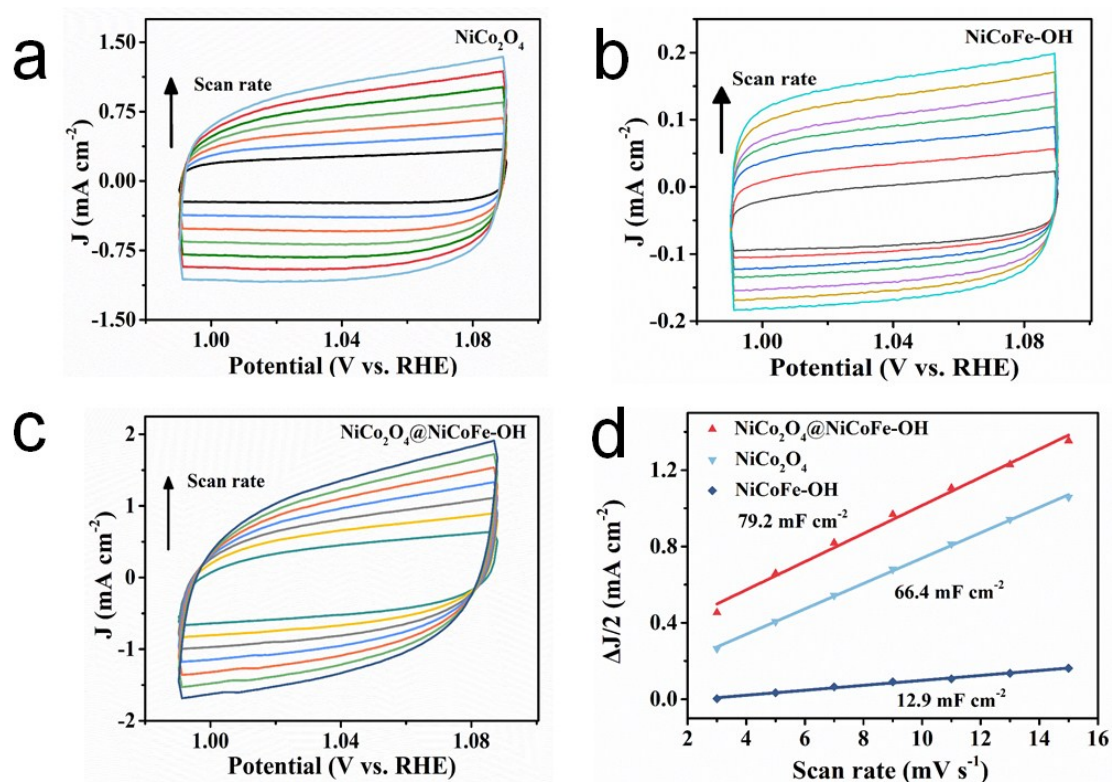
Figure S8 Cyclic voltammetry curves in the double-layer region of NiCo$_2$O$_4$ (a), NiCoFe-OH (b) and NiCo$_2$O$_4$@NiCoFe-OH (c) at scan rate of 3, 5, 7, 9, 11, 13 and 15 mV s^{-1} (along the arrow direction), respectively. (d) Half of the capacitive current difference at 1.04 V (vs. RHE) as a function of the scan rate.
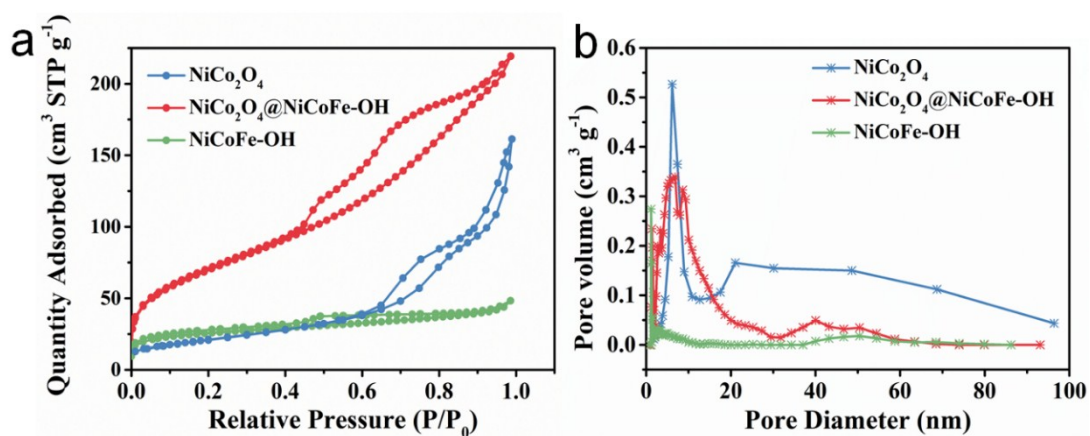
Figure S9 (a) N_2 adsorption/desorption isotherms (a) and BJH pore size distribution (b) of $NiCo_2O_4$, $NiCo_2O_4@NiCoFe-OH$ and NiCoFe-OH, respectively.

Table S3 BET surface area, pore volume and pore size of the different electrocatalysts.

Catalysts	BET surface area ($m^2\,g^{-1}$)	Pore volume ($cm^3\,g^{-1}$)	Average pore diameter (nm)
$NiCo_2O_4$	76.76	0.25	9.89
$NiCo_2O_4@NiCoFe-OH$	247.6	0.34	5.01
NiCoFe-OH	78.63	0.05	4.32
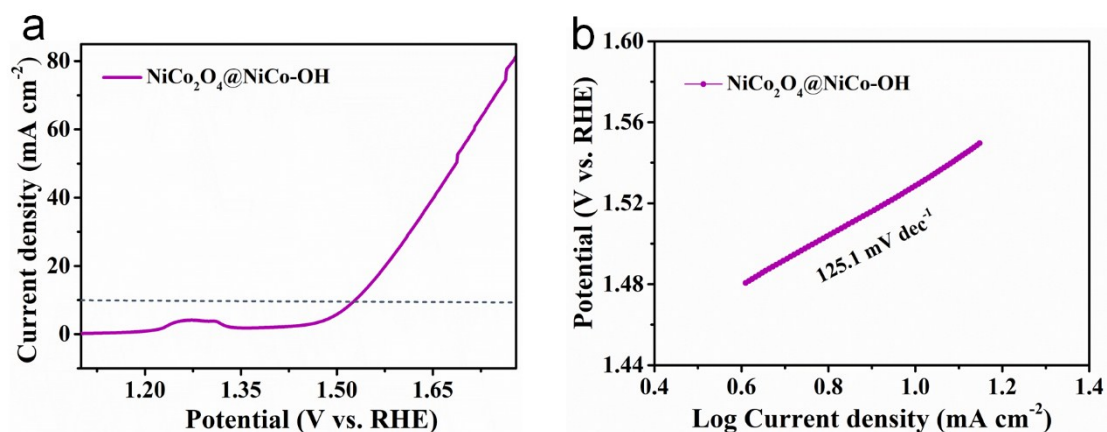
Figure S10 (a) Linear sweep voltammetry curve of $NiCo_2O_4@NiCo$-OH for OER collected in 1 M KOH at a scan rate of 1 mV s^{-1}. (b) Tafel slope of $NiCo_2O_4@NiCo$-OH.

The synthesis of $NiCo_2O_4@NiCo$-OH was basically the same to that of $NiCo_2O_4@NiCoFe$-OH except iron nitrate was not added. $NiCo_2O_4@NiCo$-OH delivers an onset overpotential of 230 mV and OER overpotential of 298 mV at the current density of 10 mA cm^{-2}. The corresponding Tafel slope of $NiCo_2O_4@NiCo$-OH is 125.1 mV dec^{-1}, much higher than that of $NiCo_2O_4@NiCoFe$-OH. Both of the significantly reduced overpotential and lower Tafel slope of $NiCo_2O_4@NiCoFe$-OH compared to $NiCo_2O_4@NiCo$-OH indicate the positive role of Fe^{3+} species in the trimetal-hydroxides layer for enhanced OER activity and catalytic kinetic.

S-14

Table S4 Electrocatalytic properties of $NiCo_2O_4$, $NiCo_2O_4$@NiCoFe-OH and recently reported bifunctional catalysts for ORR and OER.

Catalysts	Half-wave potential ($E_{1/2}$, mV)	Potential at 10 mA cm^{-2} ($E_{j=10}$, mV)	Potential difference between $E_{1/2}$ and $E_{j=10}$ (ΔE, mV)	Ref.
$NiCo_2O_4$@NiCoFe-OH	770	1465	695	This work
$NiCo_2O_4$	750	1581	831	This work
CoS_x/Co, N-Co doped CNTs	800	1540	740	[S12]
MnO/Co/Porous graphitic carbon	780	1537	757	[S13]
NiCo^{III}Fe-LDH/N-GO	778	1547	769	[S2]
$NiCo_2S_4$/N-doped CNTs	800	1600	800	[S14]
Ni_3Fe-N/C	780	1620	842	[S15]
Co@Co_3O_4/NC-1 (in CNT-grafted N-doped carbon polyhedral)	800	1650	850	[S16]
Co_3O_4/Co-N-rGO	791	1660	869	[S5]
$NiCo_2O_4$@N-doped GO	750	1630	880	[S17]

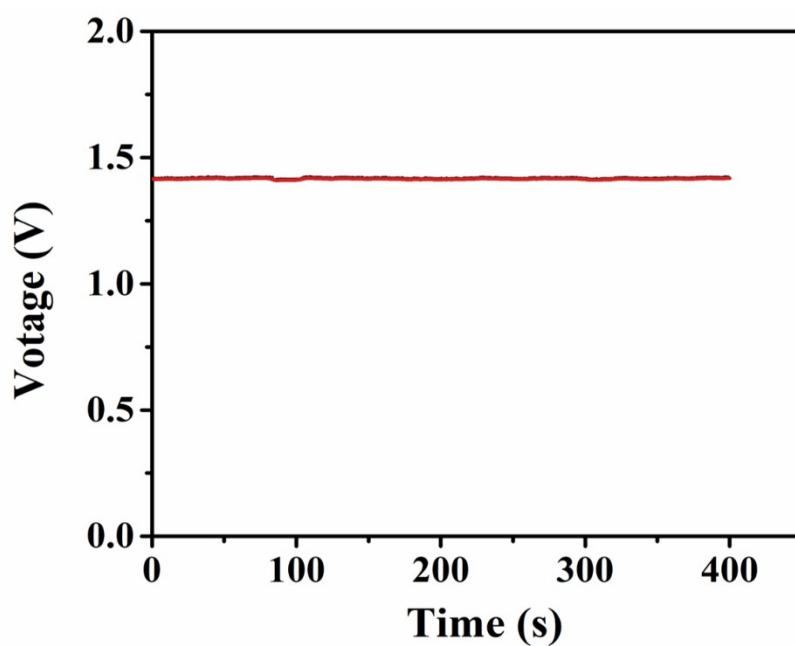|				
Ni$_x$Co$_{3-x}$O$_4$ nanosheets @Ni foil	768	1760	992	[S18]

Figure S11 Open circuit voltage of the aqueous ZAB with the NiCo$_2$O$_4$@NiCoFe-OH cathode.

Table S5 Comparison of the Open circuit voltage, specific capacity, energy density of aqueous Zn-air batteries with the $NiCo_2O_4@NiCoFe-OH$ air electrode and recently reported Zn-air batteries.

Catalysts	Loading (mg cm^{-2})	Open circuit voltage (V)	Specific capacity (mAh g$_{Zn}^{-1}$)	Energy density (Wh kg$_{Zn}^{-1}$)	Current density (mA cm^{-2})	Ref.
$NiCo_2O_4$ @NiCoFe-OH	1.02	1.42	740 / 720	864 / 767	5 / 10	This work
$NiCo_2S_4$/N-doped CNTs	1.0	1.49	431	554.6	10	[S14]
$NiCo_2S_4$ @g-C$_3$N$_4$-CNT	2.33	1.45	485.7	----	10	[S19]
CoO-NiO-NiCo	0.53	----	594	713	7	[S20]
Ni$_3$Fe/N-C	0.13	----	528	634	10	[S15]
CoZn-NC-700	0.24	----	578	694	10	[S21]
$NiCo_2O_4$ @NiMn LDH	2.0 ± 0.2	1.4	675	762	10	[S9]
ZnCo$_2$O$_4$ quantum dots/NCNT	2.0	1.47	428	595	10	[S22]
NiFe nanoparticles /N-Graphene	1	----	583	732	10	[S23]
NiO/CoN Porous nanowires	0.2	1.46	648	836	10	[S24]
Fe$_{0.5}$Co$_{0.5}$O$_x$/N-doped rGO	1	1.43	756	904	10	[S25]
CoCo$_3$O$_4$@N-doped active carbon	1.3	1.449	721	----	10	[S26]
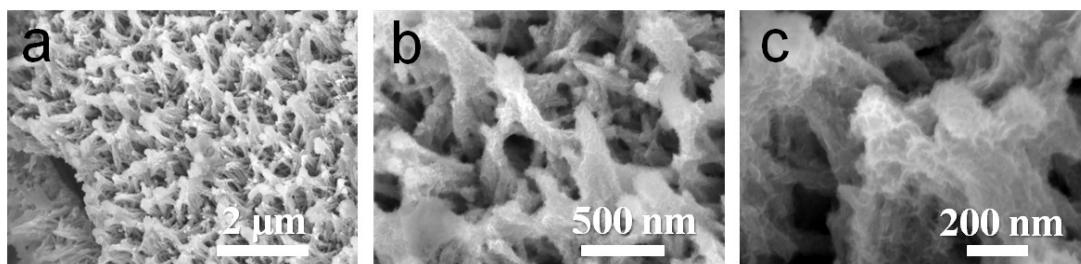
Figure S12 SEM morphology (a) and high-magnification SEM images (b, c) of the NiCo$_2$O$_4$@NiCoFe-OH binder-free cathode after intensive 500 charge/discharge cycles at a current density of 10 mA cm^{-2}.
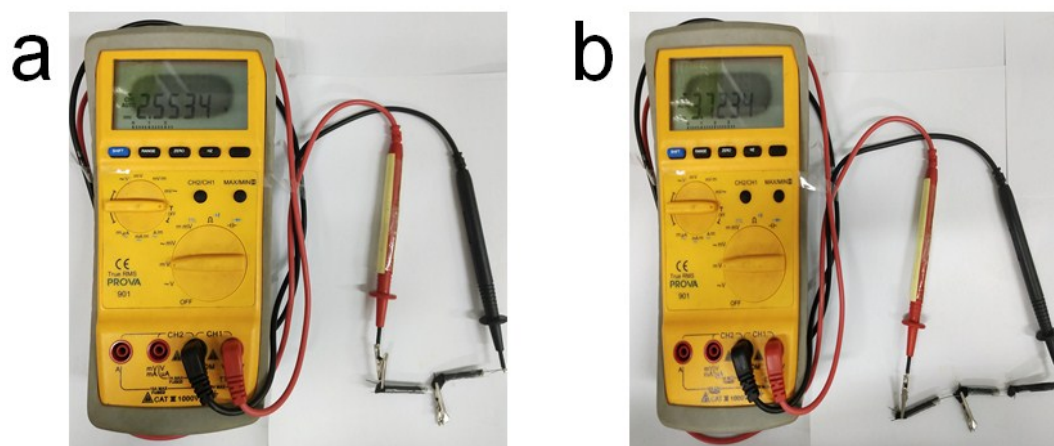
Figure S13 Optical photos showing the voltage generated by two in-series (a) and three in-series (b) cable-type batteries.
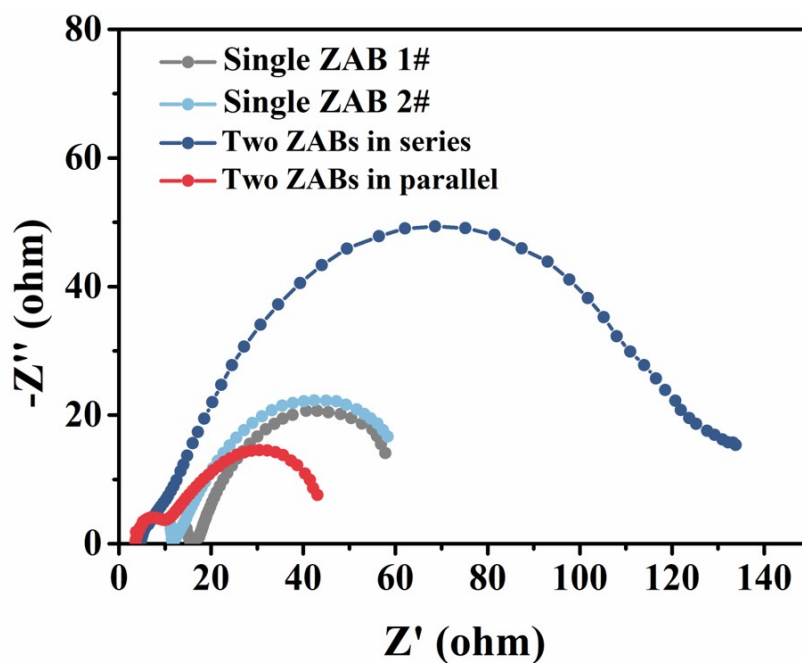
Figure S14 Nyquist plots of the cable-type zinc-air batteries (ZABs) through different connections.

Table S6 Comparison of the energy density of recently reported fiber-shaped or cable-type batteries.

Fiber or cable-shaped energy storage devices	Cathode Anode	Energy density mW h cm^{-3}	Ref.
Lithium-ion batteries (LIBs)	CNT/LiMn$_2$O$_4$ CNT/Li$_4$Ti$_5$O$_{12}$	17.7	[S27]
	(Ni–Sn)–Cu LiCoO$_2$–Al	20.4	[S28]
	LiFePO$_4$-CF Li$_4$Ti$_5$O$_{12}$	6	[S29]
Ni–Zn battery	Ni–NiO fiber Zn fiber	0.67	[S30]

Ni/Co-Zn battery	NCHO@yarn Zn@yarn	8	[S31]
Aqueous lithium-ion battery (ALIB)	$LiMn_2O_4$/CNT PI/CNT	14.3	[S32]
Sodium-ion battery (SB)	$CNT/Na_{0.44}MnO_2$ $NaTi_2(PO_4)_3$@C	25.7	[S33]
Metal-organic frameworks material-based battery (MOF)	NiZnCoP/CNTF Fe_2O_3/OCNTF	30.6	[S34]
Superiorcapacitors (SCs)	CNT/rGO composite fiber	2.4	[S35]
	Hollow rGO/PEDOT:PSS	3.2	[S36]
Zinc-air batteries (ZABs)	Co_3O_4/N-rGO Zinc wire	36.1	[S37]
	CNT sheet Zinc spring	5.7	[S38]
	$NiCo_2O_4$@NiCoFe-OH Zinc spring	38.1	This work
Zn-Co battery	CC-ZnO@C-Zn $Co(CO_3)_{0.5}(OH)_x \cdot 0.11H_2O$@CoMoO$_4$	4.6	[S39]

Video S1 Two in-series cable-type ZABs are connected and bent to light the LEDs.

Video S2 Two cable-type ZABs can power the "SCAU" panel consisting of 47 commercial green LEDs under highly distorted conditions.

References

[S1] Q. Qian, Y. Li, Y. Liu, L. Yu, G. Zhang, Ambient Fast Synthesis and Active Sites Deciphering of Hierarchical Foam-Like Trimetal-Organic Framework Nanostructures as a Platform for Highly Efficient Oxygen Evolution Electrocatalysis, *Adv. Mater*. 31 (**2019**) 1901139.

[S2] D. Zhou, Z. Cai, X. Lei, W. Tian, Y. Bi, Y. Jia, N. Han, T. Gao, Q. Zhang, Y. Kuang, J. Pan, X. Sun, X. Duan, NiCoFe-Layered Double Hydroxides/N-Doped Graphene Oxide Array Colloid Composite as an Efficient Bifunctional Catalyst for Oxygen Electrocatalytic Reactions, *Adv. Energy Mater*. 8 (**2018**) 1701905.

[S3] X. Jia, S. Gao, T. Liu, D. Li, P. Tang, Y. Feng, Fabrication and Bifunctional Electrocatalytic Performance of Ternary CoNiMn Layered Double Hydroxides/Polypyrrole/Reduced Graphene Oxide Composite for Oxygen Reduction and Evolution Reactions, *Electrochim. Acta* 245 (**2017**) 59-68.

[S4] J. Di, H. Zhu, J. Xia, J. Bao, P. Zhang, S.Z. Yang, H. Li, S. Dai, High-performance electrolytic oxygen evolution with a seamless armor core-shell FeCoNi oxynitride, *Nanoscale* 11 (**2019**) 7239-7246.

[S5] Y. Hao, Y. Xu, J. Liu, X. Sun, Nickel–cobalt oxides supported on Co/N decorated graphene as an excellent bifunctional oxygen catalyst, *J. Mater. Chem. A* 5 (**2017**) 5594-5600.

[S6] X. Yan, K. Li, L. Lyu, F. Song, J. He, D. Niu, L. Liu, X. Hu, X. Chen, From Water Oxidation to Reduction: Transformation from NixCo3-xO4 Nanowires to NiCo/NiCoOx Heterostructures, *ACS Appl. Mater. Interfaces* 8 (**2016**) 3208-3214.

[S7] J. Bao, X. Zhang, B. Fan, J. Zhang, M. Zhou, W. Yang, X. Hu, H. Wang, B. Pan, Y. Xie, Ultrathin Spinel-Structured Nanosheets Rich in Oxygen Deficiencies for Enhanced Electrocatalytic Water Oxidation, *Angew. Chem. Int. Ed.* 54 (**2015**) 7399-7404.

[S8] H. Hu, B. Guan, B. Xia, X.W. Lou, Designed Formation of $Co_3O_4/NiCo_2O_4$ Double-Shelled Nanocages with Enhanced Pseudocapacitive and Electrocatalytic Properties, *J. Am. Chem. Soc.* 137 (**2015**) 5590-5595.

[S9] X. Guo, T. Zheng, G. Ji, N. Hu, C. Xu, Y. Zhang, Core/shell design of efficient electrocatalysts based on $NiCo_2O_4$ nanowires and NiMn LDH nanosheets for rechargeable zinc–air batteries, *J. Mater. Chem. A* 6 (**2018**) 10243-10252.

[S10] S. Zeng, X. Tong, S. Zhou, B. Lv, J. Qiao, Y. Song, M. Chen, J. Di, Q. Li, All-in-One Bifunctional Oxygen Electrode Films for Flexible Zn-Air Batteries, *Small* 14 (**2018**) 1803409.

[S11] X. Zhao, Y. Fu, J. Wang, Y. Xu, J.-H. Tian, R. Yang, Ni-doped $CoFe_2O_4$ Hollow Nanospheres as Efficient Bi-functional Catalysts, *Electrochim. Acta* 201 (**2016**) 172-178.

[S12] Q. Lu, J. Yu, X. Zou, K. Liao, P. Tan, W. Zhou, M. Ni, Z. Shao, Self‐Catalyzed Growth of Co, N‐Codoped CNTs on Carbon‐Encased CoS_x Surface: A Noble‐Metal‐Free Bifunctional Oxygen Electrocatalyst for Flexible Solid Zn–Air Batteries, *Adv. Funct. Mater.* 29 (**2019**) 1904481.

[S13] X.F. Lu, Y. Chen, S. Wang, S. Gao, X.W.D. Lou, Interfacing Manganese Oxide and Cobalt in Porous Graphitic Carbon Polyhedrons Boosts Oxygen Electrocatalysis for Zn-Air Batteries, *Adv. Mater.* 31 (**2019**) 1902339.

[S14] X. Han, X. Wu, C. Zhong, Y. Deng, N. Zhao, W. Hu, $NiCo_2S_4$ nanocrystals anchored on nitrogen-doped carbon nanotubes as a highly efficient bifunctional electrocatalyst for rechargeable zinc-air batteries, *Nano Energy* 31 (**2017**) 541-550.

[S15] G. Fu, Z. Cui, Y. Chen, Y. Li, Y. Tang, J.B. Goodenough, Ni_3Fe-N Doped Carbon Sheets as a Bifunctional Electrocatalyst for Air Cathodes, *Adv. Energy Mater.* 7 (**2017**) 1601172.

[S16] A. Aijaz, J. Masa, C. Rosler, W. Xia, P. Weide, A.J. Botz, R.A. Fischer, W. Schuhmann, M. Muhler, Co@Co_3O_4 Encapsulated in Carbon Nanotube-Grafted Nitrogen-Doped Carbon Polyhedra as an Advanced Bifunctional Oxygen Electrode, *Angew. Chem. Int. Ed.* 55 (**2016**) 4087-4091.

[S17] P. Moni, S. Hyun, A. Vignesh, S. Shanmugam, Chrysanthemum flower-like $NiCo_2O_4$-nitrogen doped graphene oxide composite: an efficient electrocatalyst for

lithium-oxygen and zinc-air batteries, *Chem. Commun.* 53 (**2017**) 7836-7839.

[S18] T.N. Lambert, J.A. Vigil, S.E. White, D.J. Davis, S.J. Limmer, P.D. Burton, E.N. Coker, T.E. Beechem, M.T. Brumbach, Electrodeposited $Ni_xCo_{3-x}O_4$ nanostructured films as bifunctional oxygen electrocatalysts, *Chem. Commum.* 51 (**2015**) 9511-9514.

[S19] X. Han, W. Zhang, X. Ma, C. Zhong, N. Zhao, W. Hu, Y. Deng, Identifying the Activation of Bimetallic Sites in $NiCo_2S_4$@g-C_3N_4-CNT Hybrid Electrocatalysts for Synergistic Oxygen Reduction and Evolution, *Adv. Mater.* 31 (**2019**) 1808281.

[S20] X. Liu, M. Park, M.G. Kim, S. Gupta, G. Wu, J. Cho, Integrating NiCo Alloys with Their Oxides as Efficient Bifunctional Cathode Catalysts for Rechargeable Zinc-Air Batteries, *Angew. Chem. Int. Ed.* 54 (**2015**) 9654-9658.

[S21] B. Chen, X. He, F. Yin, H. Wang, D.-J. Liu, R. Shi, J. Chen, H. Yin, MO-Co@N-Doped Carbon (M = Zn or Co): Vital Roles of Inactive Zn and Highly Efficient Activity toward Oxygen Reduction/Evolution Reactions for Rechargeable Zn-Air Battery, *Adv. Funct. Mater.* 27 (**2017**) 1700795.

[S22] Z.Q. Liu, H. Cheng, N. Li, T.Y. Ma, Y.Z. Su, $ZnCo_2O_4$ Quantum Dots Anchored on Nitrogen-Doped Carbon Nanotubes as Reversible Oxygen Reduction/Evolution Electrocatalysts, *Adv. Mater.* 28 (**2016**) 3777-3784.

[S23] J. Zhu, M. Xiao, Y. Zhang, Z. Jin, Z. Peng, C. Liu, S. Chen, J. Ge, W. Xing, Metal–Organic Framework-Induced Synthesis of Ultrasmall Encased NiFe Nanoparticles Coupling with Graphene as an Efficient Oxygen Electrode for a Rechargeable Zn–Air Battery, *ACS Catal.* 6 (**2016**) 6335-6342.

[S24] J. Yin, Y. Li, F. Lv, Q. Fan, Y.Q. Zhao, Q. Zhang, W. Wang, F. Cheng, P. Xi, S. Guo, NiO/CoN Porous Nanowires as Efficient Bifunctional Catalysts for Zn-Air Batteries, *ACS Nano* 11 (**2017**) 2275-2283.

[S25] L. Wei, H.E. Karahan, S. Zhai, H. Liu, X. Chen, Z. Zhou, Y. Lei, Z. Liu, Y. Chen, Amorphous Bimetallic Oxide-Graphene Hybrids as Bifunctional Oxygen Electrocatalysts for Rechargeable Zn-Air Batteries, *Adv. Mater.* 29 (**2017**) 1701410.

[S26] X. Zhong, W. Yi, Y. Qu, L. Zhang, H. Bai, Y. Zhu, J. Wan, S. Chen, M. Yang, L. Huang, M. Gu, H. Pan, B. Xu, Co single-atom anchored on Co_3O_4 and nitrogen-

doped active carbon toward bifunctional catalyst for zinc-air batteries, *Appl. Catal. B* 260 (**2020**) 118188.

[S27] J. Ren, Y. Zhang, W. Bai, X. Chen, Z. Zhang, X. Fang, W. Weng, Y. Wang, H. Peng, Elastic and wearable wire-shaped lithium-ion battery with high electrochemical performance, *Angew. Chem. Int. Ed.* 53 (**2014**) 7864-7869.

[S28] Y.H. Kwon, S.W. Woo, H.R. Jung, H.K. Yu, K. Kim, B.H. Oh, S. Ahn, S.Y. Lee, S.W. Song, J. Cho, H.C. Shin, J.Y. Kim, Cable-type flexible lithium ion battery based on hollow multi-helix electrodes, *Adv. Mater.* 24 (**2012**) 5192-5197.

[S29] F. Mo, G. Liang, Z. Huang, H. Li, D. Wang, C. Zhi, An Overview of Fiber-Shaped Batteries with a Focus on Multifunctionality, Scalability, and Technical Difficulties, *Adv. Mater.* (**2019**) 1902151.

[S30] Y. Zeng, Y. Meng, Z. Lai, X. Zhang, M. Yu, P. Fang, M. Wu, Y. Tong, X. Lu, An Ultrastable and High-Performance Flexible Fiber-Shaped Ni-Zn Battery based on a Ni-NiO Heterostructured Nanosheet Cathode, *Adv. Mater*. 29 (**2017**) 1702698.

[S31] Y. Huang, W.S. Ip, Y.Y. Lau, J. Sun, J. Zeng, N.S.S. Yeung, W.S. Ng, H. Li, Z. Pei, Q. Xue, Y. Wang, J. Yu, H. Hu, C. Zhi, Weavable, Conductive Yarn-Based NiCo//Zn Textile Battery with High Energy Density and Rate Capability, *ACS Nano* 11 (**2017**) 8953-8961.

[S32] Y. Zhang, Y. Wang, L. Wang, C.-M. Lo, Y. Zhao, Y. Jiao, G. Zheng, H. Peng, A fiber-shaped aqueous lithium ion battery with high power density, *J. Mater. Chem. A* 4 (**2016**) 9002-9008.

[S33] Z. Guo, Y. Zhao, Y. Ding, X. Dong, L. Chen, J. Cao, C. Wang, Y. Xia, H. Peng, Y. Wang, Multi-functional Flexible Aqueous Sodium-Ion Batteries with High Safety, *Chem* 3 (**2017**) 348-362.

[S34] Q. Zhang, Z. Zhou, Z. Pan, J. Sun, B. He, Q. Li, T. Zhang, J. Zhao, L. Tang, Z. Zhang, L. Wei, Y. Yao, All-Metal-Organic Framework-Derived Battery Materials on Carbon Nanotube Fibers for Wearable Energy-Storage Device, *Adv. Sci.* 5 (**2018**) 1801462.

[S35] B. Wang, X. Fang, H. Sun, S. He, J. Ren, Y. Zhang, H. Peng, Fabricating

Continuous Supercapacitor Fibers with High Performances by Integrating All Building Materials and Steps into One Process, *Adv. Mater.* 27 (**2015**) 7854-7860.

[S36] G. Qu, J. Cheng, X. Li, D. Yuan, P. Chen, X. Chen, B. Wang, H. Peng, A Fiber Supercapacitor with High Energy Density Based on Hollow Graphene/Conducting Polymer Fiber Electrode, *Adv. Mater.* 28 (**2016**) 3646-3652.

[S37] Y. Li, C. Zhong, J. Liu, X. Zeng, S. Qu, X. Han, Y. Deng, W. Hu, J. Lu, Atomically Thin Mesoporous Co_3O_4 Layers Strongly Coupled with N-rGO Nanosheets as High-Performance Bifunctional Catalysts for 1D Knittable Zinc-Air Batteries, *Adv. Mater*. 30 (**2018**) 1703657.

[S38] Y. Xu, Y. Zhang, Z. Guo, J. Ren, Y. Wang, H. Peng, Flexible, Stretchable, and Rechargeable Fiber-Shaped Zinc-Air Battery Based on Cross-Stacked Carbon Nanotube Sheets, *Angew. Chem. Int. Ed.* 54 (**2015**) 15390-15394.

[S39] M. Li, J. Meng, Q. Li, M. Huang, X. Liu, K.A. Owusu, Z. Liu, L. Mai, Finely Crafted 3D Electrodes for Dendrite-Free and High-Performance Flexible Fiber-Shaped Zn-Co Batteries, *Adv. Funct. Mater.* 28 (**2018**) 1802016.